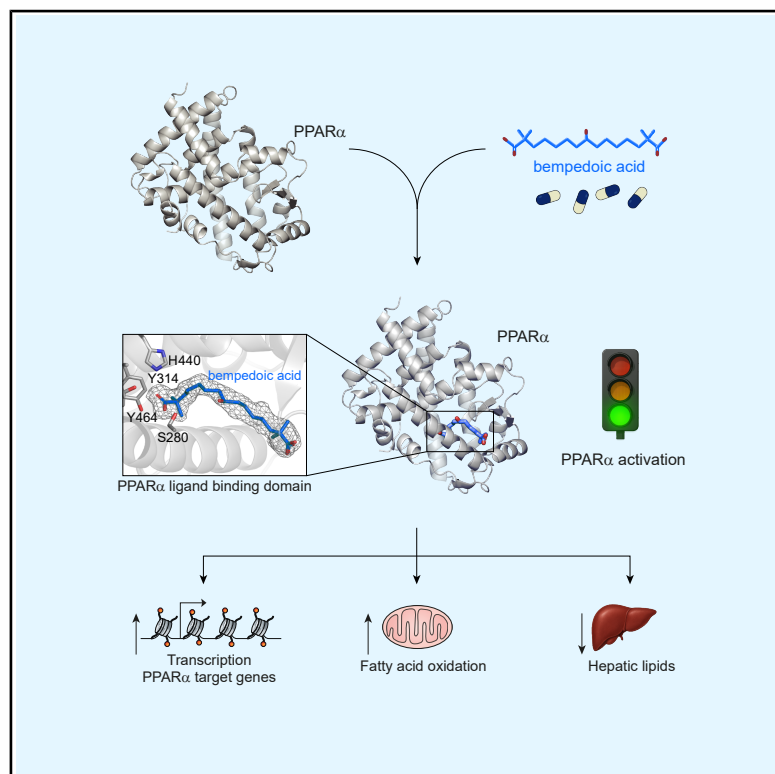


## Bempedoic acid directly binds and activates PPAR $\alpha$

### Graphical abstract



### Authors

Christina Papa, Alina Rose, Hugo N.G. Martin, ..., Georg Künze, John T. Heiker, Bilal N. Sheikh

### Correspondence

bilal.sheikh@helmholtz-munich.de

### In brief

Bempedoic acid is a recently approved drug that lowers cholesterol and lipids. Papa et al. show that bempedoic acid directly binds to and activates PPAR $\alpha$  to enhance fatty acid oxidation, revealing the mechanistic basis for its lipid-lowering effects.

### Highlights

- BA directly activates PPAR $\alpha$  and its transcriptional networks
- BA binds to the ligand-binding domain of PPAR $\alpha$  and stabilizes its active state
- BA activates PPAR $\alpha$  networks independently of ACSVL1
- BA requires PPAR $\alpha$  to stimulate fatty acid oxidation

Short article

# Bempedoic acid directly binds and activates PPAR $\alpha$

Christina Papa,<sup>1,19</sup> Alina Rose,<sup>1,19</sup> Hugo N.G. Martin,<sup>1,19</sup> Abibe Useini,<sup>2</sup> Florian Geier,<sup>1</sup> Longsheng Liao,<sup>1</sup> Jesús Rafael Rodríguez-Aguilera,<sup>1</sup> Philipp Valina-Allo,<sup>1</sup> Anne Hoffmann,<sup>1</sup> Andrey Tvardovskiy,<sup>3</sup> Faiqa Zulfqar,<sup>1</sup> Andrea Zimmerman,<sup>4</sup> Gerda Schicht,<sup>4</sup> Fritz Ott,<sup>5,6</sup> Christiane Körner,<sup>5,6</sup> Beatrice Engelmann,<sup>7</sup> Ulrike Rolle-Kampczyk,<sup>7</sup> Martin von Bergen,<sup>7,8,9</sup> Matthias Meier,<sup>10,11</sup> Till Bartke,<sup>3</sup> Daniel Seehofer,<sup>4</sup> Nora Klötting,<sup>1</sup> Madlen Matz-Soja,<sup>5,6</sup> Georg Damm,<sup>4</sup> Jes-Niels Boeckel,<sup>12</sup> Joerg M. Buescher,<sup>13</sup> Matthias Blüher,<sup>1,14</sup> Ulrich Laufs,<sup>12</sup> Olga Bondareva,<sup>1</sup> Norbert Sträter,<sup>15</sup> Georg Künze,<sup>2,16,17</sup> John T. Heiker,<sup>1</sup> and Bilal N. Sheikh<sup>1,18,20,\*</sup>

<sup>1</sup>Helmholtz Institute for Metabolic, Obesity and Vascular Research (HI-MAG), Helmholtz Center Munich, 04103 Leipzig, Germany

<sup>2</sup>Institute for Drug Discovery, Medical Faculty, Leipzig University, 04103 Leipzig, Germany

<sup>3</sup>Institute of Functional Epigenetics (IFE), Helmholtz Munich, 85764 Neuherberg, Germany

<sup>4</sup>Department of Hepatobiliary Surgery and Visceral Transplantation, University Hospital of Leipzig, Leipzig 04103, Germany

<sup>5</sup>Rudolf-Schönheimer Institute for Biochemistry, Faculty of Medicine, Leipzig University, 04103 Leipzig, Germany

<sup>6</sup>Division of Hepatology, Clinic of Oncology, Gastroenterology, Hepatology and Pneumology, University Hospital Leipzig, 04103 Leipzig, Germany

<sup>7</sup>Helmholtz-Centre for Environmental Research-UFZ GmbH, Department for Molecular Toxicology, 04318 Leipzig, Germany

<sup>8</sup>German Centre for Integrative Biodiversity Research (iDiv), Halle-Jena-Leipzig, Puschstraße 4, 04103 Leipzig, Germany

<sup>9</sup>Functional Proteomics, University of Leipzig, Faculty of Life Sciences, Institute of Biochemistry, Brüderstraße 34, 04103 Leipzig, Germany

<sup>10</sup>Helmholtz Pioneer Campus, Helmholtz Munich, 85764 Neuherberg, Germany

<sup>11</sup>Centre for Biotechnology and Biomedicine, University of Leipzig, 04103 Leipzig, Germany

<sup>12</sup>Klinik und Poliklinik für Kardiologie, Universitätsklinikum Leipzig, 04103 Leipzig, Germany

<sup>13</sup>Max Planck Institute of Immunobiology and Epigenetics, Stübeweg 51, 79108 Freiburg im Breisgau, Germany

<sup>14</sup>Clinic for Endocrinology, Nephrology, and Rheumatology, Leipzig University Medical Center, Liebigstrasse 20, 04103 Leipzig, Germany

<sup>15</sup>Institute of Bioanalytical Chemistry, Centre for Biotechnology and Biomedicine, Leipzig University, Deutscher Platz 5, 04103 Leipzig, Germany

<sup>16</sup>Interdisciplinary Center for Bioinformatics, Leipzig University, 04107 Leipzig, Germany

<sup>17</sup>Center for Scalable Data Analytics and Artificial Intelligence, Leipzig University, 04105 Leipzig, Germany

<sup>18</sup>German Center for Diabetes Research (DZD), 85764 Neuherberg, Germany

<sup>19</sup>These authors contributed equally

<sup>20</sup>Lead contact

\*Correspondence: [bilal.sheikh@helmholtz-munich.de](mailto:bilal.sheikh@helmholtz-munich.de)

<https://doi.org/10.1016/j.cmet.2025.12.018>

## SUMMARY

Bempedoic acid (BA) is a recently approved drug that lowers cholesterol and hepatic lipids, yet its mechanism of action remains incompletely understood. Here, we combine transcriptomic, biochemical, and structural approaches to show that BA directly binds to and activates peroxisome proliferator-activated receptor alpha (PPAR $\alpha$ ). BA treatment robustly induced PPAR $\alpha$  signaling and fatty acid oxidation in primary hepatocytes and mouse liver. Through X-ray crystallography, we uncovered that BA binds to the ligand-binding domain of PPAR $\alpha$  and stabilizes its active conformation. BA activated PPAR $\alpha$  target genes independently of very-long-chain acyl-coenzyme A (CoA) synthetase (ACSVL1), the liver-enriched enzyme that converts BA to its bempedoyl-CoA form. Notably, BA-mediated induction of fatty acid oxidation required PPAR $\alpha$ . Together, this work reveals direct PPAR $\alpha$  activation as a key mechanism of BA action, providing a molecular basis for its lipid-lowering effects and suggesting broader therapeutic potential beyond the liver.

## INTRODUCTION

Bempedoic acid (BA) is a recently approved drug that effectively lowers blood LDL cholesterol and reduces cardiovascular disease risk.<sup>1,2</sup> BA is proposed to function as a pro-drug that is activated by very-long-chain acyl-coenzyme A (CoA) synthetase (ACSVL1, also known as SLC27A2) to bempedoyl-CoA.<sup>3</sup> Bempedoyl-CoA inhibits citrate lyase (ACLY), reducing acetyl-

CoA production and thereby limiting cholesterol and fatty acid biosynthesis.<sup>3,4</sup> As ACSVL1 expression is largely confined to hepatocytes,<sup>3,4</sup> the liver is considered the primary location of BA activity and ACLY inhibition.

Recent findings suggest that BA exerts additional effects beyond ACLY inhibition.<sup>5</sup> Notably, BA reduced hepatic lipids in liver-specific *Acly* knockout mice,<sup>5</sup> which is inconsistent with ACLY being the sole target of BA. In addition to ACLY, BA has

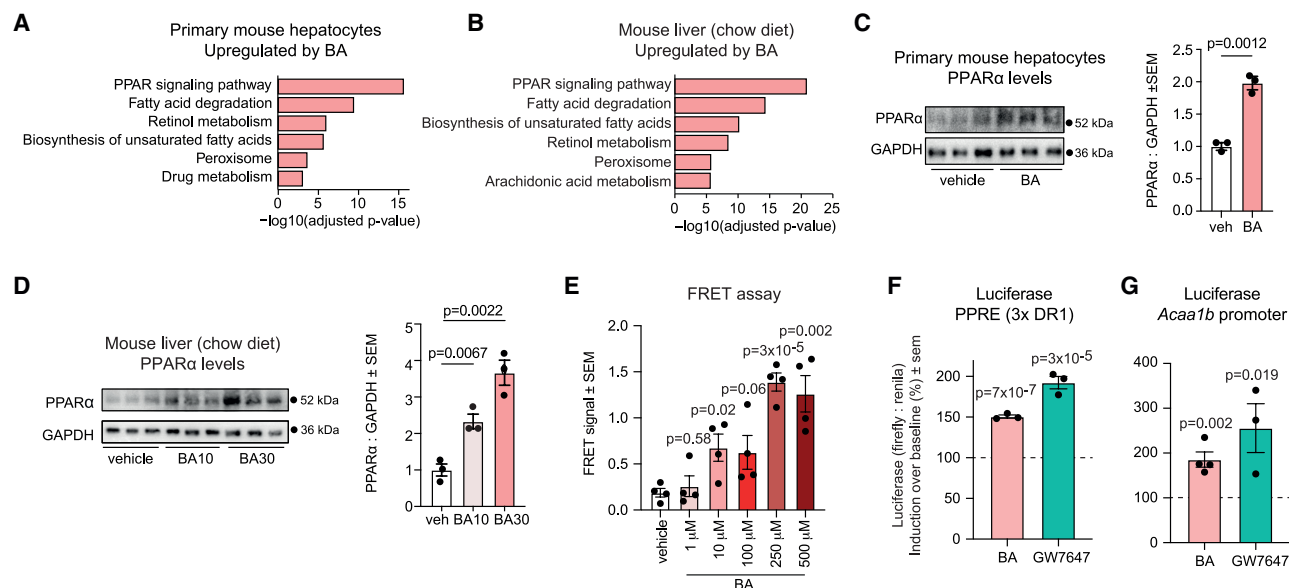


**Figure 1. BA directly activates PPAR $\alpha$**

(A) KEGG-annotated pathways most significantly activated by BA in primary mouse hepatocytes. Significantly upregulated genes (adjusted  $p < 0.05$ ,  $\log_2$  fold change  $> 0.5$ ) were used for these analyses.  $n = 4$  independent cultures per treatment group.

(B) KEGG-annotated pathways most significantly activated by BA in the liver. Mice were treated with a 30 mg/kg body weight dose of BA (BA30) daily for 4 weeks prior to analyses. Significantly upregulated genes (adjusted  $p < 0.05$ ,  $\log_2$  fold change  $> 0.5$ ) were used for these analyses.  $n = 5$  animals per group.

(C) Western blot analysis of PPAR $\alpha$  in primary mouse hepatocytes treated with 100  $\mu$ M BA and vehicle. GAPDH is provided as a loading control. Right: quantification of PPAR $\alpha$  levels relative to GAPDH signal. Data are provided as mean  $\pm$  SEM and were analyzed via a two-tailed Student's  $t$  test.  $n = 3$  independent cultures per group.

(D) Western blot analysis of PPAR $\alpha$  from mouse livers treated with vehicle and daily doses of 10 mg/kg (BA10) or 30 mg/kg BA (BA30). GAPDH is provided as a loading control. Right: western blot signal quantification. Data are provided as mean  $\pm$  SEM and were analyzed via a two-tailed Student's  $t$  test.  $n = 3$  mice per group.

(E) FRET analyses using the TR-FRET PPAR $\alpha$  coactivator assay kit. FRET signal (emission at 520 nm: 495 nm) is provided. Data are presented as mean  $\pm$  SEM and were analyzed using a two-sided Student's  $t$  test, with each treatment group compared with vehicle.  $n = 4$  replicates per group. The experiment was independently repeated three times with similar results.

(F and G) Luciferase assay: primary mouse hepatocytes were transfected with a (F) PPRE or (G) *Acaa1b* promoter reporter plasmid and treated with BA for 48 h. Firefly luciferase signal was standardized to renilla signal. Data are expressed as fold induction relative to vehicle-treated (DMSO) controls. Data are presented as mean  $\pm$  SEM and were analyzed via a two-sided Student's  $t$  test by comparing each group to vehicle controls.  $n = 3$ –4 biological replicates per group.

BA, bempedoic acid; BA10, 10 mg/kg body weight dose; BA30, 30 mg/kg body weight dose.

See also Figure S1.

been proposed to activate AMP-activated protein kinase (AMPK)<sup>3</sup> and peroxisome proliferator-activated receptor alpha (PPAR $\alpha$ ),<sup>6,7</sup> but direct evidence for these interactions is limited. Given the range of reported beneficial effects of BA beyond cholesterol reduction, such as decreasing hepatic lipids, fibrosis, and inflammation,<sup>8</sup> it is imperative to understand the molecular function of BA; this will help guide its use in patients to address health issues beyond cholesterol lowering.

In this study, we sought to address how BA mechanistically controls lipid metabolism. We provide here structural and biochemical evidence showing the direct interaction of BA with PPAR $\alpha$ , which leads to PPAR $\alpha$  activation and induction of fatty acid oxidation.

## RESULTS

### BA directly activates PPAR $\alpha$ and its transcriptional networks

As hepatocytes are the main site of BA activity, we initially undertook RNA sequencing (RNA-seq) analyses of primary mouse he-

patocytes treated with BA (Figures S1A and S1B). Our data revealed a strong activation of PPAR signaling, fatty acid degradation, and retinol metabolism pathways (Figure 1A). To extend our findings to animal models, we treated lean mice and mice with obesity with BA for 4 weeks (Figures S1C and S1D). RNA-seq analyses of the liver also revealed PPAR signaling and fatty acid degradation as the top activated pathways following BA treatment in lean and obese mice (Figures 1B and S1E). These changes were associated with increased PPAR $\alpha$  protein levels following BA treatment (Figures 1C, 1D, and S1F), which is the main PPAR-family member active in the liver. Together, our data revealed that the induction of PPAR $\alpha$  and activation of PPAR target genes were the most prominent changes following BA treatment.

Given the transcriptional activation of PPAR and lipid metabolic networks by BA, we addressed whether BA could directly activate PPAR $\alpha$ . We employed a fluorescence resonance energy transfer (FRET) assay to measure coactivator peptide recruitment to activated PPAR $\alpha$ . In this cell-free system, BA led to a concentration-dependent increase in FRET signal (Figure 1E),

indicating direct activation of PPAR $\alpha$ . To validate these findings in a cellular context, we carried out luciferase assays in primary mouse hepatocytes transfected with reporters driven by either a PPAR response element (PPRE), or the *Acaa1b* promoter, a PPAR-target gene. In both assays, BA significantly increased luciferase signal to levels comparable to the established PPAR $\alpha$  agonist GW7647 (Figures 1F and 1G). Together, these results demonstrate that BA directly activates PPAR $\alpha$ .

### BA binds to the ligand-binding domain of PPAR $\alpha$

We considered how BA could activate PPAR $\alpha$  at the molecular level. Various saturated and unsaturated fatty acids have been identified as natural PPAR $\alpha$  ligands.<sup>9</sup> BA resembles a saturated long-chain fatty acid, such as palmitic acid, which is a known ligand of PPAR $\alpha$  (Figure 2A). To determine if BA could directly interact with PPAR $\alpha$ , we undertook thermal shift assays. BA triggered a concentration-dependent shift in the melting temperature of PPAR $\alpha$  protein (Figure 2B), suggesting a physical interaction between BA and PPAR $\alpha$ .

To assess whether BA engages PPAR $\alpha$  similarly to known ligands,<sup>10</sup> we expressed and purified the ligand-binding domain of PPAR $\alpha$  (Figure S2) and solved the crystal structure of the PPAR $\alpha$  ligand-binding domain with the coactivator peptide PPAR gamma coactivator 1 alpha (PGC1 $\alpha$ ) and BA at a resolution of 1.7 Å (Figure 2C). The structure contains two copies of the PPAR $\alpha$ ×PGC1 $\alpha$ ×BA complex in the asymmetric unit, denoted as chains A and C. BA wraps around the long helix 3 (H3) of PPAR $\alpha$ , with one of the two carboxylate groups, forming hydrogen bonds with S280, Y314, H440, and Y464 (Figures 2C and 2D). H12 (red) contains Y464 and adopts the active “up” conformation when bound by BA (Figure 2C). This active state of PPAR $\alpha$  is stabilized by interactions between the carboxylate group of BA, H12, and the PGC1 $\alpha$  coactivator peptide. Additional polar groups of BA are partially solvent accessible and form hydrogen bonds with water molecules, further supporting stable binding (Figure 2E). Superposition of the two BA chains shows similar binding modes, with minor differences in the conformation of the long alkyl chain (Figure 2F), which suggests limited structural flexibility. This binding mode of BA to PPAR $\alpha$  is similar to palmitic acid, stearic acid, and tetradecylthioacetic acid<sup>10</sup> (Figure 2G). Together, these analyses reveal that BA binds in the ligand-binding pocket of PPAR $\alpha$  and stabilizes its active conformation.

### BA-mediated activation of the PPAR $\alpha$ network is independent of ACSVL1

Inhibition of ACLY by BA is currently thought to require its activation by the ACSVL1 enzyme (encoded by the *Slc27a2* gene), which converts BA to bempedoil-CoA.<sup>4</sup> We wondered if BA-mediated activation of PPAR $\alpha$  target genes also required ACSVL1 activity. We undertook RNA-seq analyses of BA-treated primary mouse hepatocytes following *Ppara* and *Slc27a2* knockdown. BA induced the expression of PPAR $\alpha$  target genes including *Acaa1b*, *Acot2*, *Cyp4a14*, *Cyp4a10*, *Ehhadh*, and *Hmgcs2* (Figures 3A and 3B). *Ppara* knockdown mitigated the induction of these genes, while *Slc27a2* knockdown had no significant impact on their expression (Figures 3A and 3B). These findings suggest that BA-driven activation of lipid metabolism genes requires PPAR $\alpha$  but is independent of ACSVL1. These observations are consistent with the FRET assay (Figure 1E) and

structural analyses (Figures 2C–2G), showing direct binding of BA to PPAR $\alpha$  in its active conformation.

A central function of PPAR $\alpha$  is to stimulate fatty acid catabolism via fatty acid oxidation. Given that BA directly binds and activates PPAR $\alpha$ , we investigated if BA could functionally modulate fatty acid metabolism via PPAR $\alpha$ . Treatment of primary mouse hepatocytes with BA increased fatty acid oxidation to levels comparable with the PPAR $\alpha$  agonist GW7647 (Figure 3C). This effect was abolished by *Ppara* knockdown (Figures 3D and 3E), suggesting that BA stimulates fatty acid oxidation in a PPAR $\alpha$ -dependent manner.

## DISCUSSION

In this study, we set out to investigate the molecular function of BA. Our data show that BA can directly interact with and activate PPAR $\alpha$ , leading to increased transcription of PPAR $\alpha$  target genes and induction of fatty acid catabolism.

Clinical trials have shown that BA reduces circulating LDL cholesterol and major cardiovascular events,<sup>1</sup> which has been attributed to BA-mediated ACLY inhibition.<sup>3,4</sup> Our data argue that in addition to ACLY inhibition, BA can directly act as a PPAR agonist. Clinical trials utilizing PPAR agonists have shown a modest reduction in total and LDL cholesterol, improved insulin sensitivity and glucose levels, and lower risk of cardiovascular diseases.<sup>11–13</sup> These reports overlap with clinical outcomes following BA treatment, suggesting that at least some improvement in metabolic health is likely driven by BA-mediated PPAR activation.

BA treatment significantly reduces inflammatory markers in patients,<sup>1</sup> and animal studies have also shown reduced liver fibrosis.<sup>8</sup> It is unclear whether these effects are driven solely by BA activity in hepatocytes, which express ACSVL1 and convert BA to bempedoil-CoA.<sup>3</sup> Our data argue that BA activates PPAR $\alpha$  independently of ACSVL1 (Figures 3A and 3B). Thus, BA could act beyond hepatocytes and stimulate PPAR $\alpha$  activity in all cell types where PPAR $\alpha$  is present, such as macrophages, renal cells, and cardiomyocytes. This model could also explain the broad reported effects of BA on fibrosis, cardiovascular, and metabolic health. While we have explored the effects of BA on PPAR $\alpha$  in hepatocytes, it is plausible that BA may also have some activity on PPAR $\gamma$  and PPAR $\delta$ , which remains to be addressed.

In sum, we here present evidence of direct binding and activation of PPAR $\alpha$  by BA, which is likely to extend the activity of BA beyond the liver. Our data highlight the promise of BA to treat a range of metabolic disorders driven by lipid dyshomeostasis.

### Limitations of the study

In this study, we uncovered that BA requires PPAR $\alpha$ , but not ACSVL1, to activate lipid metabolic networks in primary cell culture models. As the liver is considered the main site of BA activity,<sup>3</sup> we conducted our mechanistic analyses with *Slc27a2* and *Ppara* knockdowns in primary mouse hepatocytes. However, additional work is needed to understand the functional importance of the BA-PPAR $\alpha$  axis for lipid lowering,<sup>1</sup> moderating inflammation,<sup>14</sup> and reducing fibrosis<sup>8</sup> *in vivo*. Studies using models such as *Slc27a2* knockout, *Ppara* knockout, and liver-specific *Ppara* knockouts treated with BA are required to determine if the mechanisms uncovered in this study also hold true *in vivo*.

BA is currently used clinically for cholesterol lowering, a function that is attributed to BA-mediated ACLY inhibition.<sup>3,4,15</sup>

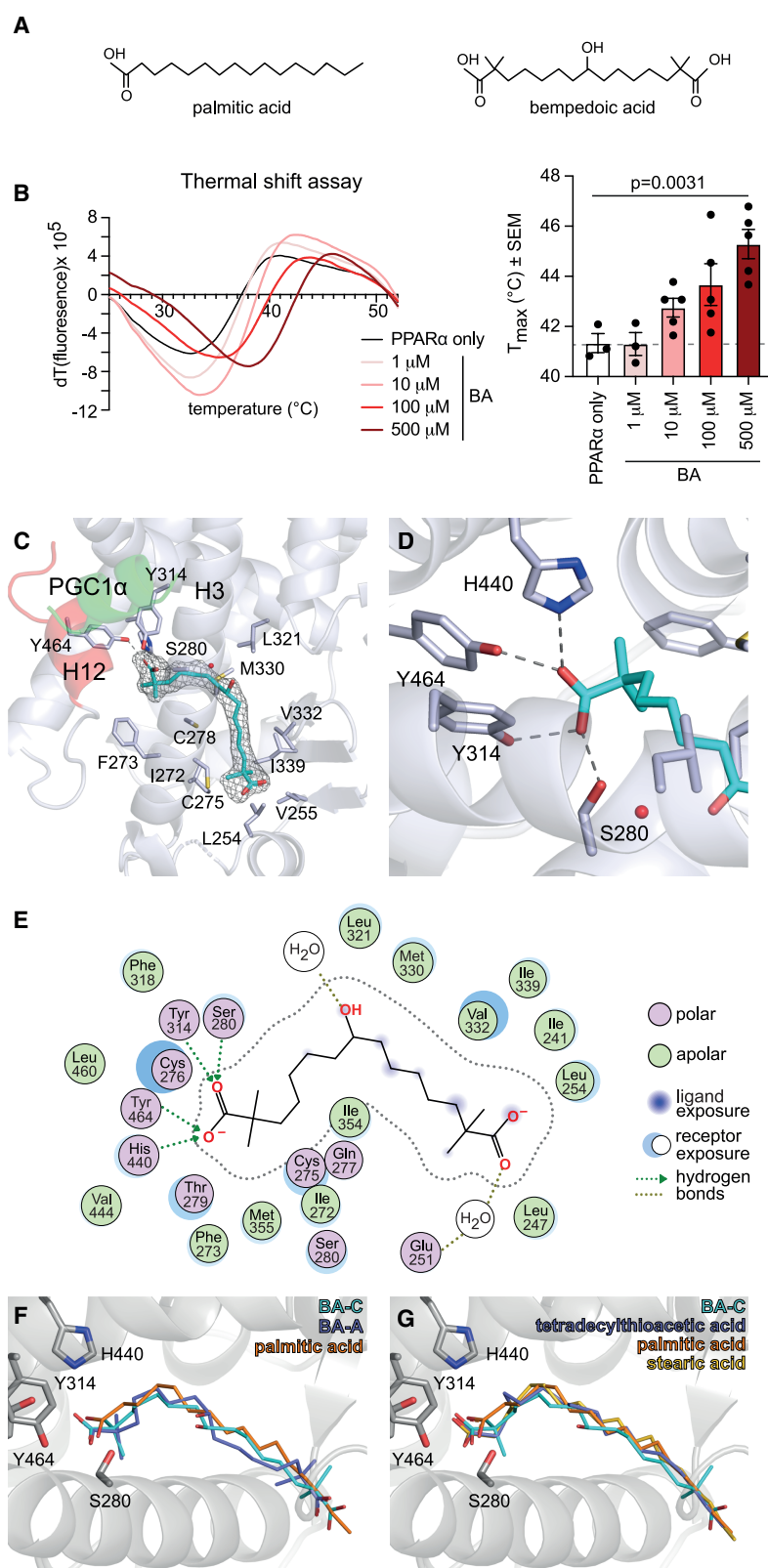


**Figure 2. BA binds to the ligand-binding domain of PPAR $\alpha$**

(A) Chemical structures of palmitic acid and BA. (B) Thermal shift assay displaying PPAR $\alpha$  protein melting curves in the presence of BA. Right: temperature at which the maximum ( $T_{\text{max}}$ ) dT (fluorescence) signal was observed. Data are presented as mean  $\pm$  SEM and were analyzed using a two-sided Student's  $t$  test.  $n = 5$  for 500, 100, and 10  $\mu\text{M}$  concentrations of BA;  $n = 3$  for 1  $\mu\text{M}$  BA and PPAR $\alpha$ -only controls. (C) Crystal structure of BA bound to PPAR $\alpha$ . H12 is colored in red and the coactivator peptide PGC1 $\alpha$  in green. The cartoon fold is represented in transparency. H3 is in front of the ligand in this view. The polder omit electron density map (gray mesh) is contoured at 3  $\sigma_{\text{rms}}$ . (D) Hydrogen bonding interactions of the BA carboxylate group binding next to H12. (E) Scheme of the binding mode. The intensity of the blue circles next to the protein residues or behind ligand atoms indicates the solvent accessibility. (F) Superposition of the two BA binding modes observed in the crystal structure of PPAR $\alpha$  chains A and C (PDB: 9T5S) and the binding mode of palmitic acid (PDB: 6lx6). (G) Comparison of the BA binding mode (chain C) to those of palmitic acid (PDB: 6lx6),<sup>10</sup> stearic acid (PDB: 6lx7),<sup>10</sup> and tetradecylthioacetic acid (PDB: 6kb1).<sup>10</sup> BA, bempedoic acid; H3, helix 3; H12, helix 12; KD, knockdown; PGC1 $\alpha$ , PPAR gamma coactivator 1 alpha. See also Figure S2.

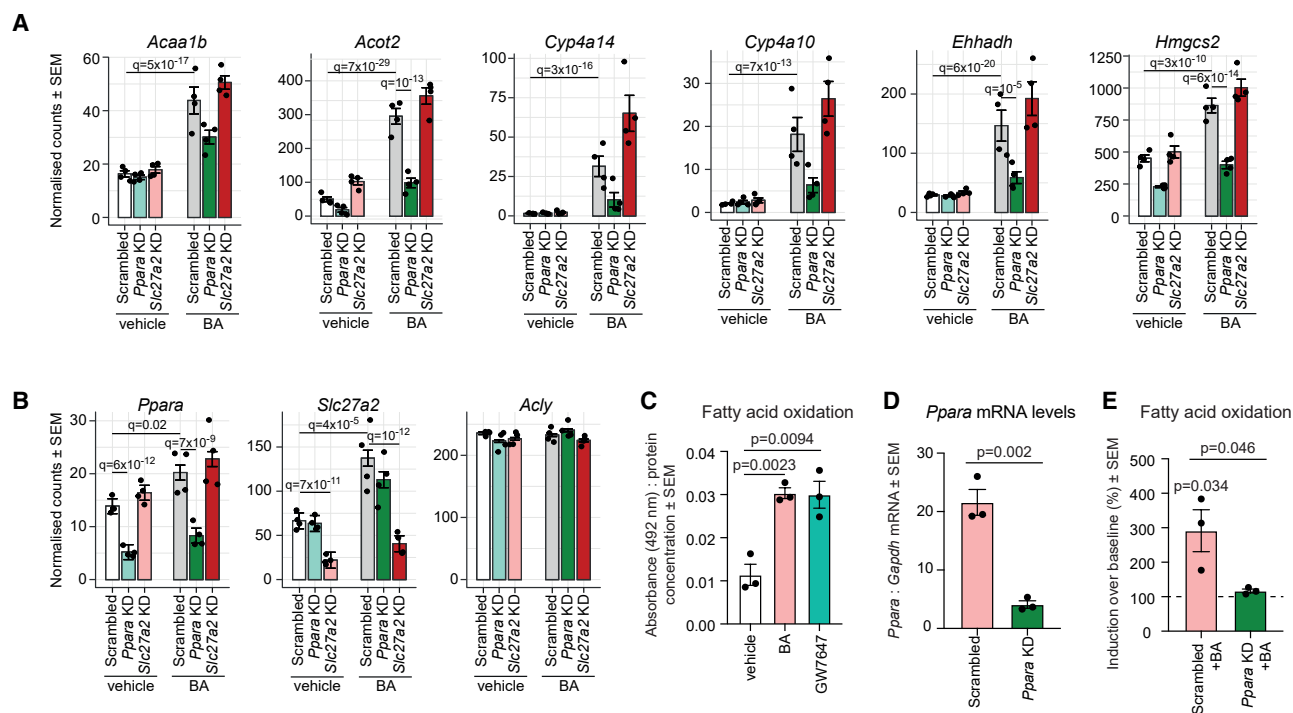


**Figure 3. BA activates the PPAR $\alpha$  network independently of ACSVL1**

(A) Normalized transcript levels of PPAR $\alpha$ -target genes *Acaa1b*, *Acot2*, *Cyp4a14*, *Cyp4a10*, *Ehhadh*, and *Hmgcs2*, following treatment with 100  $\mu$ M BA and siRNA-mediated *Ppara* or *Slc27a2* KD. Data are shown as mean  $\pm$  SEM. Statistics were generated using the DE-Seq2 pipeline.  $n = 4$  independent cultures per group.

(B) Normalized transcript levels of *Ppara*, *Slc27a2*, and *Acly* after KD of *Ppara* and *Slc27a2*. Data were analyzed via RNA-seq. Data are shown as mean  $\pm$  SEM. Statistics were generated using the DE-Seq2 pipeline.  $n = 4$  independent cultures per group.

(C) Quantification of fatty acid oxidation levels, following treatment with BA or the established PPAR $\alpha$  agonist GW7647. Data are presented as mean  $\pm$  SEM and were analyzed via a two-sided Student's  $t$  test comparing each treatment group with vehicle controls.  $n = 3$  biological replicates (independent primary mouse hepatocyte cultures) per group.

(D) RT-qPCR data quantifying changes in *Ppara* mRNA following siRNA-mediated KD in primary mouse hepatocytes. Data are presented as mean  $\pm$  SEM and were analyzed by a two-sided Student's  $t$  test.  $n = 3$  biological replicates per group.

(E) Quantification of fatty acid oxidation levels, following treatment with BA and *Ppara* KD. Data are presented as fold induction over vehicle (DMSO)-treated controls. Data are presented as mean  $\pm$  SEM and were analyzed via a two-sided Student's  $t$  test.  $n = 3$  biological replicates (independent primary mouse hepatocyte cultures) per group.

BA, bempedoic acid; KD, knockdown; q, adjusted  $p$  value.

However, PPAR $\alpha$  agonists such as fibrates also reduce circulating LDL cholesterol levels.<sup>12</sup> In this study, we did not dissect the relative contribution of ACLY inhibition versus PPAR $\alpha$  activation to the cholesterol-lowering effects of BA. Furthermore, whether BA is active in tissues beyond the liver, as suggested by our results, needs to be tested in primary cell culture and animal models. Addressing these gaps will help clarify the molecular mechanism of BA action and potentially broaden its scope for clinical use beyond cholesterol lowering.

## RESOURCE AVAILABILITY

### Lead contact

Inquiries regarding resources, reagents, and further information should be directed to and will be fulfilled by the lead contact, Bilal Sheikh ([bilal.sheikh@helmholtz-munich.de](mailto:bilal.sheikh@helmholtz-munich.de)).

### Materials availability

All unique reagents generated in this study are available from the lead contact without restriction.

## Data and code availability

- The raw RNA-seq data from this study have been uploaded to Zenodo and are available under the following records: primary mouse hepatocytes (PMHs)—control Zenodo: 14774048, PMH + BA: 14774109; chow-fed animals—vehicle: 10497820, BA30: 10497880; Western diet-fed animals—vehicle: 17831524, BA30: 17831551; *Ppara* and *Slc27a2* knockdown (KD) experiment—Scramble small interfering RNA (siRNA) + vehicle: 15526474, Scramble siRNA + BA: 15526797, *Ppara* siRNA + vehicle: 15527025, *Ppara* siRNA + BA: 15527316, *Slc27a2* siRNA + vehicle: 15527494, *Slc27a2* siRNA + BA: 15527704.
- The structure of PPAR $\alpha$  with BA has been uploaded to PDB under ID PDB: 9T5S.
- Raw data and uncropped western blots can be found in [Data S1](#).

## ACKNOWLEDGMENTS

We are grateful to Daniela Kern and Marlene Hausner for technical support and to Konstanze Julich-Gruner, Susanne Renno, and Sandra Zentile for administrative help. We thank Marcela Sosa-Garrocho, Carlos Peralta Álvarez (UNAM, Mexico City), and Maria Shvedunova (Max Planck Institute, Freiburg) for their advice and helpful discussions. We acknowledge the EMBL beamlines of the

DESY synchrotron in Hamburg for synchrotron beamtime. We further thank Dr. Renato Weiße and Michael Agthe for their support during data collection. This work was supported by the Deutsche Forschungsgemeinschaft (DFG) project grants (457240345 and 511049882 awarded to B.N.S.), SFB1052 (project number 209933838, subprojects B1 to M.B., B4 to N.K., and C7 to J.T.H.) and SFB1382 (project number 403224013, subproject B5 to M.v.B.), the European Union's EIC Pathfinder Programme (grant no. 101130454 [ISOS] supporting A.U. and G.K.), the Matomic Project - Novo Nordisk Foundation (grant number NNF21OC0066551 to M.v.B. and B.E.), and funding from the German Center for Diabetes Research (DZD), free-state of Saxony and Helmholtz Munich.

## AUTHOR CONTRIBUTIONS

A.R., U.L., and B.N.S. conceptualized, initiated, and developed the project. C.P., A.R., A.U., F.G., L.L., J.R.R.-A., P.V.-A., F.Z., G.S., F.O., C.K., B.E., U.R.-K., J.M.B., and J.T.H. undertook the experiments. C.P., A.U., F.G., N.S., and J.T.H. did the crystal structure analyses. H.N.G.M., A.H., A.T., and O.B. undertook bioinformatics analyses. M.v.B., M.M., T.B., D.S., M.M.S., G.D., J.-N.B., J.M.B., M.B., U.L., N.S., G.K., J.T.H., and B.N.S. supervised the project. C.P., A.R., F.G., and N.K. undertook the animal studies. B.N.S. acquired funding for the project. C.P., A.R., and B.N.S. wrote the paper. All authors read, edited, and approved the manuscript.

## DECLARATION OF INTERESTS

M.B. received honoraria as a consultant and speaker from Amgen, AstraZeneca, Bayer, Boehringer Ingelheim, Lilly, Novo Nordisk, Novartis, and Sanofi.

## STAR★METHODS

Detailed methods are provided in the online version of this paper and include the following:

- **KEY RESOURCES TABLE**
- **EXPERIMENTAL MODEL AND STUDY PARTICIPANT DETAILS**
- **METHOD DETAILS**
  - BA treatment - animals
  - Histology
  - Primary mouse hepatocyte culture
  - siRNA mediated knockdowns
  - Immunoblotting
  - RNA Sequencing
  - Sequencing data pre-processing
  - Differential gene expression and gene set enrichment analyses
  - Thermal shift assay
  - Fatty Acid Oxidation (FAO) Assay
  - TR-FRET Peroxisome Proliferator Receptor  $\alpha$  Coactivator Assay
  - Luciferase Assay
  - PPAR $\alpha$  expression and purification
  - Coomassie staining
  - Crystal Structure Determination
- **QUANTIFICATION AND STATISTICAL ANALYSIS**

## SUPPLEMENTAL INFORMATION

Supplemental information can be found online at <https://doi.org/10.1016/j.cmet.2025.12.018>.

Received: May 9, 2025

Revised: November 7, 2025

Accepted: December 16, 2025

## REFERENCES

1. Nissen, S.E., Lincoff, A.M., Brennan, D., Ray, K.K., Mason, D., Kastelein, J.J.P., Thompson, P.D., Libby, P., Cho, L., Plutzky, J., et al. (2023). Bempedoic acid and cardiovascular outcomes in statin-intolerant patients. *N. Engl. J. Med.* 388, 1353–1364. <https://doi.org/10.1056/NEJMoa2215024>.
2. Banach, M., Duell, P.B., Gotto, A.M., Jr., Laufs, U., Leiter, L.A., Mancini, G.B.J., Ray, K.K., Flaim, J., Ye, Z., and Catapano, A.L. (2020). Association of bempedoic acid administration with atherogenic lipid levels in phase 3 randomized clinical trials of patients with hypercholesterolemia. *JAMA Cardiol.* 5, 1124–1135. <https://doi.org/10.1001/jamacardio.2020.2314>.
3. Pinkosky, S.L., Filippov, S., Srivastava, R.A.K., Hanselman, J.C., Bradshaw, C.D., Hurley, T.R., Cramer, C.T., Spahr, M.A., Brant, A.F., Houghton, J.L., et al. (2013). AMP-activated protein kinase and ATP-citrate lyase are two distinct molecular targets for ETC-1002, a novel small molecule regulator of lipid and carbohydrate metabolism. *J. Lipid Res.* 54, 134–151. <https://doi.org/10.1194/jlr.M030528>.
4. Pinkosky, S.L., Newton, R.S., Day, E.A., Ford, R.J., Lhotak, S., Austin, R.C., Birch, C.M., Smith, B.K., Filippov, S., Groot, P.H.E., et al. (2016). Liver-specific ATP-citrate lyase inhibition by bempedoic acid decreases LDL-C and attenuates atherosclerosis. *Nat. Commun.* 7, 13457. <https://doi.org/10.1038/ncomms13457>.
5. Liu, J.Y., Kuna, R.S., Pinheiro, L.V., Nguyen, P.T.T., Welles, J.E., Drummond, J.M., Murali, N., Sharma, P.V., Supplee, J.G., Shiue, M., et al. (2024). Bempedoic acid suppresses diet-induced hepatic steatosis independently of ATP-citrate lyase. *Cell Metab.* 37, 239–254.e7. <https://doi.org/10.1016/j.cmet.2024.10.014>.
6. Bentanachs, R., Velázquez, A.M., Sánchez, R.M., Alegret, M., Laguna, J.C., and Roglans, N. (2022). Bempedoic acid as a PPAR $\alpha$  activator: new perspectives for hepatic steatosis treatment in a female rat experimental model. *Clin. Investig. Arterioscler.* 34, 57–67. <https://doi.org/10.1016/j.arteri.2021.09.004>.
7. Xie, Z., Cheng, L., Hu, Y., Song, G., Wang, F., Zhang, M., Zhang, Y., Zhang, X., Zhou, C., Zhu, X., et al. (2025). The enedioic acid analog 326E alleviates metabolic dysfunction-associated steatohepatitis via dual targeting at ACLY and PPAR $\alpha$ . *Cell Metab.* 37, 2149–2166.e9. <https://doi.org/10.1016/j.cmet.2025.09.011>.
8. Morrow, M.R., Batchuluun, B., Wu, J., Ahmadi, E., Leroux, J.M., Mohammadi-Shemirani, P., Desjardins, E.M., Wang, Z., Tsakiridis, E.E., Lavoie, D.C.T., et al. (2022). Inhibition of ATP-citrate lyase improves NASH, liver fibrosis, and dyslipidemia. *Cell Metab.* 34, 919–936.e8. <https://doi.org/10.1016/j.cmet.2022.05.004>.
9. Xu, H.E., Lambert, M.H., Montana, V.G., Parks, D.J., Blanchard, S.G., Brown, P.J., Sternbach, D.D., Lehmann, J.M., Wisely, G.B., Willson, T.M., et al. (1999). Molecular recognition of fatty acids by peroxisome proliferator-activated receptors. *Mol. Cell* 3, 397–403. [https://doi.org/10.1016/S1097-2765\(00\)80467-0](https://doi.org/10.1016/S1097-2765(00)80467-0).
10. Kamata, S., Oyama, T., Saito, K., Honda, A., Yamamoto, Y., Suda, K., Ishikawa, R., Itoh, T., Watanabe, Y., Shibata, T., et al. (2020). PPAR $\alpha$  ligand-binding domain structures with endogenous fatty acids and fibrates. *iScience* 23, 101727. <https://doi.org/10.1016/j.isci.2020.101727>.
11. Cariou, B., Hanf, R., Lambert-Porcheron, S., Zaïr, Y., Sauvinet, V., Noël, B., Flet, L., Vidal, H., Staels, B., and Laville, M. (2013). Dual peroxisome proliferator-activated receptor  $\alpha/\delta$  agonist GFT505 improves hepatic and peripheral insulin sensitivity in abdominally obese subjects. *Diabetes Care* 36, 2923–2930. <https://doi.org/10.2337/dc12-2012>.
12. Abourbih, S., Fillion, K.B., Joseph, L., Schiffrin, E.L., Rinfret, S., Poirier, P., Pilote, L., Genest, J., and Eisenberg, M.J. (2009). Effect of fibrates on lipid profiles and cardiovascular outcomes: a systematic review. *Am. J. Med.* 122, 962.e1–962.e8. <https://doi.org/10.1016/j.amjmed.2009.03.030>.
13. Francque, S.M., Bedossa, P., Ratzliff, V., Anstee, Q.M., Bugianesi, E., Sanyal, A.J., Loomba, R., Harrison, S.A., Balabanska, R., Mateva, L., et al. (2021). A randomized, controlled trial of the pan-PPAR agonist

- lanifibrinor in NASH. *N. Engl. J. Med.* 385, 1547–1558. <https://doi.org/10.1056/NEJMoa2036205>.
14. Stroes, E.S.G., Bays, H.E., Banach, M., Catapano, A.L., Duell, P.B., Laufs, U., Mancini, G.B.J., Ray, K.K., Sasiela, W.J., Zhang, Y., et al. (2023). Bempedoic acid lowers high-sensitivity C-reactive protein and low-density lipoprotein cholesterol: Analysis of pooled data from four phase 3 clinical trials. *Atherosclerosis* 373, 1–9. <https://doi.org/10.1016/j.atherosclerosis.2023.03.020>.
15. Pinkosky, S.L., Groot, P.H.E., Lalwani, N.D., and Steinberg, G.R. (2017). Targeting ATP-citrate lyase in hyperlipidemia and metabolic disorders. *Trends Mol. Med.* 23, 1047–1063. <https://doi.org/10.1016/j.molmed.2017.09.001>.
16. Krueger, F., James, F., Ewels, P., Afyounian, E., Weinstein, M., Schuster-Boeckler, B., Hulsemans, G., and sclamons. (2023). FelixKrueger/TrimGalore: v0.6.10 - add default decompression path. Zenodo. <https://doi.org/10.5281/zenodo.7598955>.
17. Dobin, A., Davis, C.A., Schlesinger, F., Drenkow, J., Zaleski, C., Jha, S., Batut, P., Chaisson, M., and Gingeras, T.R. (2013). STAR: ultrafast universal RNA-seq aligner. *Bioinformatics* 29, 15–21. <https://doi.org/10.1093/bioinformatics/bts635>.
18. Danecek, P., Bonfield, J.K., Liddle, J., Marshall, J., Ohan, V., Pollard, M.O., Whitwham, A., Keane, T., McCarthy, S.A., Davies, R.M., et al. (2021). Twelve years of SAMtools and BCFtools. *GigaScience* 10, giab008. <https://doi.org/10.1093/gigascience/giab008>.
19. Wang, L., Wang, S., and Li, W. (2012). RSeQC: quality control of RNA-seq experiments. *Bioinformatics* 28, 2184–2185. <https://doi.org/10.1093/bioinformatics/bts356>.
20. Ewels, P., Magnusson, M., Lundin, S., and Käller, M. (2016). MultiQC: summarize analysis results for multiple tools and samples in a single report. *Bioinformatics* 32, 3047–3048. <https://doi.org/10.1093/bioinformatics/btw354>.
21. Love, M.I., Huber, W., and Anders, S. (2014). Moderated estimation of fold change and dispersion for RNA-seq data with DESeq2. *Genome Biol.* 15, 550. <https://doi.org/10.1186/s13059-014-0550-8>.
22. Chen, E.Y., Tan, C.M., Kou, Y., Duan, Q., Wang, Z., Meirelles, G.V., Clark, N.R., and Ma'ayan, A. (2013). Enrichr: interactive and collaborative HTML5 gene list enrichment analysis tool. *BMC Bioinform.* 14, 128. <https://doi.org/10.1186/1471-2105-14-128>.
23. Zhu, A., Ibrahim, J.G., and Love, M.I. (2019). Heavy-tailed prior distributions for sequence count data: removing the noise and preserving large differences. *Bioinformatics* 35, 2084–2092. <https://doi.org/10.1093/bioinformatics/bty895>.
24. Kabsch, W. (2010). Xds. *Acta Crystallogr. D Biol. Crystallogr.* 66, 125–132. <https://doi.org/10.1107/S0907444909047337>.
25. Vonnrhein, C., Tickle, I.J., Flensburg, C., Keller, P., Paciorek, W., Sharff, A., and Bricogne, G. (2018). Advances in automated data analysis and processing within autoPROC, combined with improved characterisation, mitigation and visualisation of the anisotropy of diffraction limits using STARANISO. *Acta Crystallogr. A Found. Adv.* 74, a360. <https://doi.org/10.1107/S010876731809640X>.
26. Delagenière, S., Brenchereau, P., Launer, L., Ashton, A.W., Leal, R., Veyrier, S., Gabadinho, J., Gordon, E.J., Jones, S.D., Levik, K.E., et al. (2011). ISPyB: an information management system for synchrotron macromolecular crystallography. *Bioinformatics* 27, 3186–3192. <https://doi.org/10.1093/bioinformatics/btr535>.
27. Liebschner, D., Afonine, P.V., Baker, M.L., Bunkóczi, G., Chen, V.B., Croll, T.I., Hintze, B., Hung, L.W., Jain, S., McCoy, A.J., et al. (2019). Macromolecular structure determination using X-rays, neutrons and electrons: recent developments in Phenix. *Acta Crystallogr. D Struct. Biol.* 75, 861–877. <https://doi.org/10.1107/S2059798319011471>.
28. Emsley, P., Lohkamp, B., Scott, W.G., and Cowtan, K. (2010). Features and development of Coot. *Acta Crystallogr., D* 66, 486–501. <https://doi.org/10.1107/S0907444910007493>.
29. Samsoondar, J.P., Burke, A.C., Sutherland, B.G., Telford, D.E., Sawyez, C.G., Edwards, J.Y., Pinkosky, S.L., Newton, R.S., and Huff, M.W. (2017). Prevention of diet-induced metabolic dysregulation, inflammation, and atherosclerosis in *Ldlr*<sup>-/-</sup> mice by treatment with the ATP-citrate lyase inhibitor bempedoic acid. *Arterioscler. Thromb. Vasc. Biol.* 37, 647–656. <https://doi.org/10.1161/ATVBAHA.116.308963>.
30. Frankish, A., Diekhans, M., Jungreis, I., Lagarde, J., Loveland, J.E., Mudge, J.M., Sisu, C., Wright, J.C., Armstrong, J., Barnes, I., et al. (2021). GENCODE 2021. *Nucleic Acids Res.* 49, D916–D923. <https://doi.org/10.1093/nar/gkaa1087>.
31. Liao, Y., Smyth, G.K., and Shi, W. (2014). featureCounts: an efficient general purpose program for assigning sequence reads to genomic features. *Bioinformatics* 30, 923–930. <https://doi.org/10.1093/bioinformatics/btt656>.
32. Kim, J.B., Wright, H.M., Wright, M., and Spiegelman, B.M. (1998). ADD1/SREBP1 activates PPARgamma through the production of endogenous ligand. *Proc. Natl. Acad. Sci. USA* 95, 4333–4337. <https://doi.org/10.1073/pnas.95.8.4333>.
33. Noske, G.D., Nakamura, A.M., Gawriljuk, V.O., Fernandes, R.S., Lima, G. M.A., Rosa, H.V.D., Pereira, H.D., Zeri, A.C.M., Nascimento, A.F.Z., Freire, M.C.L.C., et al. (2021). A crystallographic snapshot of SARS-CoV-2 main protease maturation process. *J. Mol. Biol.* 433, 167118. <https://doi.org/10.1016/j.jmb.2021.167118>.
34. Xu, H.E., Lambert, M.H., Montana, V.G., Plunket, K.D., Moore, L.B., Collins, J.L., Oplinger, J.A., Kliewer, S.A., Gampe, R.T., Jr., McKee, D. D., et al. (2001). Structural determinants of ligand binding selectivity between the peroxisome proliferator-activated receptors. *Proc. Natl. Acad. Sci. USA* 98, 13919–13924. <https://doi.org/10.1073/pnas.241410198>.

## STAR★METHODS

### KEY RESOURCES TABLE

REAGENT or RESOURCE	SOURCE	IDENTIFIER
<b>Antibodies</b>		
PPAR $\alpha$	Abcam	Cat# ab126285; RRID: AB_3073567
GAPDH	ThermoFisher	Cat# A300-641A; RRID: AB_513619
peroxidase conjugated anti-rabbit	GE healthcare	Cat# GENA934; RRID: AB_2722659
His-tag HRP conjugated	Santa Cruz	Cat# sc-8036; RRID: AB_627727
<b>Bacterial and virus strains</b>		
DH5 $\alpha$	Life Technologies	18263012
BL21 Rosetta2	Sigma Aldrich	71397
<b>Chemicals, peptides, and recombinant proteins</b>		
Bempedoic acid	Cayman Chemical	26409
GW7647	Sigma Aldrich	G6793
Liver Perfusion Kit mouse & rat	Miltenyi Biotec	130-128-030
GST-tagged human PPAR alpha protein	Thermo Fisher	PV4692
<b>Critical commercial assays</b>		
Protein Thermal Shift kit	Thermo Fisher	4461146
Fatty Acid Oxidation Assay Kit	Assay Genie	BR00001
LanthaScreen TR-FRET PPAR $\alpha$ Coactivator Assay Kit	Thermo Fisher	PV4684
Firefly/Renilla Dual Luciferase Assay	Sigma Aldrich	SCT152
<b>Deposited data</b>		
RNA-Seq primary mouse hepatocytes (female) control	This paper	Zenodo: <a href="https://zenodo.org/record/14774047">10.5281/zenodo.14774047</a>
RNA-Seq primary mouse hepatocytes (female) BA	This paper	Zenodo: <a href="https://zenodo.org/record/14774109">10.5281/zenodo.14774109</a>
RNA-Seq in vivo vehicle (liver) – chow diet	This paper	Zenodo: <a href="https://zenodo.org/record/10497820">10.5281/zenodo.10497820</a>
RNA-Seq in vivo BA30 (liver) – chow diet	This paper	Zenodo: <a href="https://zenodo.org/record/10497880">10.5281/zenodo.10497880</a>
RNA-Seq in vivo vehicle (liver) – Western diet	This paper	Zenodo: <a href="https://zenodo.org/record/17831524">10.5281/zenodo.17831524</a>
RNA-Seq in vivo BA30 (liver) – Western diet	This paper	Zenodo: <a href="https://zenodo.org/record/17831551">10.5281/zenodo.17831551</a>
RNA-Seq Scramble siRNA + vehicle	This paper	Zenodo: <a href="https://zenodo.org/record/15526474">10.5281/zenodo.15526474</a>
RNA-Seq Scramble siRNA + BA	This paper	Zenodo: <a href="https://zenodo.org/record/15526797">10.5281/zenodo.15526797</a>
RNA-Seq <i>Ppara</i> siRNA + vehicle	This paper	Zenodo: <a href="https://zenodo.org/record/15527025">10.5281/zenodo.15527025</a>
RNA-Seq <i>Ppara</i> siRNA + BA	This paper	Zenodo: <a href="https://zenodo.org/record/15527316">10.5281/zenodo.15527316</a>
RNA-Seq <i>Slc27a2</i> siRNA + vehicle	This paper	Zenodo: <a href="https://zenodo.org/record/15527494">10.5281/zenodo.15527494</a>
RNA-Seq <i>Slc27a2</i> siRNA + BA	This paper	Zenodo: <a href="https://zenodo.org/record/15527704">10.5281/zenodo.15527704</a>
PPAR $\alpha$ - BA structure	This paper	PDB: 9T5S
PPAR $\alpha$ – palmitic acid structure	Kamata et al. <sup>10</sup>	PDB: 6lx6
PPAR $\alpha$ – stearic acid structure	Kamata et al. <sup>10</sup>	PDB: 6lx7
PPAR $\alpha$ – tetradecylioacetic acid structure	Kamata et al. <sup>10</sup>	PDB: 6kb1
<a href="#">Data S1</a>	This paper	Raw data
<b>Experimental models: Organisms/strains</b>		
C57BL6/NTac mice	In house breeding	N/A
<b>Oligonucleotides</b>		
Mouse <i>Ppara</i> siRNA	Horizon	L-040740-01-0005
Mouse <i>Slc27a2</i> siRNA	Horizon	L-048371-01-0005
Non-targeting siRNA pool	Horizon	D-001810-10-05
<i>Ppara</i> forward qRT-PCR primer; AGACAAAGAGGCAGAGGTC	This paper	N/A
<i>Ppara</i> reverse qRT-PCR primer; AAGGAGGACAGCATCGTGAA	This paper	N/A

(Continued on next page)

### Continued

REAGENT or RESOURCE	SOURCE	IDENTIFIER
<i>Gapdh</i> forward qRT-PCR primer; TTCACCACCATGGAGAAGGC	This paper	N/A
<i>Gapdh</i> reverse qRT-PCR primer; CCCTTTGGCTCCACCCT	This paper	N/A
<b>Recombinant DNA</b>		
PPRE X3-TK-luc	Addgene	#1015
<i>Acaa1b</i> promoter luciferase reporter	This study	N/A
<i>Ppara</i> wild type cDNA (pET28a-Ndel-wt PPAR $\alpha$ )	This study	N/A
pGL4.23 [hRluc/TK]	Promega	E6921
<b>Software and algorithms</b>		
Trim Galore v.0.6.10	Krueger et al. <sup>16</sup>	N/A
STAR v.2.7.10b	Dobin et al. <sup>17</sup>	N/A
Samtools	Danecek et al. <sup>18</sup>	N/A
RSeQC	Wang et al. <sup>19</sup>	N/A
MultiQC	Ewels et al. <sup>20</sup>	N/A
DESeq2 (v1.36.0)	Love et al. <sup>21</sup>	N/A
enrichR	Chen et al. <sup>22</sup>	N/A
apeglim	Zhu et al. <sup>23</sup>	N/A
XDS	Kabsch <sup>24</sup>	N/A
STARANISO	Vonrhein et al. <sup>25</sup>	N/A
ISPyB	Delagenière et al. <sup>26</sup>	N/A
Phenix	Liebschner et al. <sup>27</sup>	N/A
Coot	Emsley et al. <sup>28</sup>	N/A
Pymol	<a href="https://pymol.org">https://pymol.org</a>	N/A
<b>Other</b>		
Chow diet	Ssniff Spezialdiäten	V1534
Western diet	Ssniff Spezialdiäten	D12331

## EXPERIMENTAL MODEL AND STUDY PARTICIPANT DETAILS

All experiments were performed in accordance with the animal ethics laws of Saxony, Germany, and were approved by the state animal ethics committee (Landesdirektion Sachsen, Leipzig, Germany) under the ethics numbers TVV05/23, T06/21, T09/21 and T14/23. Animals were provided with ad libitum access to water and food. The study room was maintained at a temperature of 21–24°C and relative humidity at 40–70%. The animal rooms were maintained under 12 h light and dark cycle. Animals were maintained on a C57BL/6N background.

## METHOD DETAILS

### BA treatment - animals

Male C57BL/6N mice were put on a Western diet (Ssniff Spezialdiäten GmbH D12331, <https://www.ssniff.com/>, under Surwit diets) or control chow diet (Ssniff Spezialdiäten GmbH V1534) starting at 8 weeks of age. Animals were maintained on the respective diets for 12 weeks and weighed weekly (Figure S1C). Animals under the different diets were randomized at 20 weeks of age, and grouped to receive either vehicle (0.5% w/v methyl cellulose and 0.5% v/v Tween 80), BA 10 mg per kg body weight<sup>8,29</sup> or BA 30 mg per kg body weight<sup>4,8,29</sup> via oral gavage for a period of 30 days. Body composition analysis was performed on the first and last days of treatment with BA via the EchoMRI™ minispec LF110 (Bruker). Serum was obtained during sacrifice for analyses. Liver was dissected directly after death, cut into small pieces, and processed for analyses.

### Histology

The liver was cut into approximately 0.5 cm<sup>3</sup> pieces and fixed with 4% formaldehyde overnight at 4°C. Tissues were embedded in paraffin, and 6  $\mu$ m sections were cut using a microtome (Thermo Scientific, HM355S) and attached to Superfrost slides (Epredia, J1800AMNZ). After deparaffinization and rehydration, sections were incubated in 50% hematoxylin (Sigma Aldrich, 1.05175.0500) for 5 min and washed afterwards with 0.02% ammonium hydroxide (Sigma Aldrich, 221228) and H<sub>2</sub>O. Eosin (0.1%) staining was performed for 2 min. Representative images were taken with the Keyence BZ-X800 microscope.

### Primary mouse hepatocyte culture

Primary mouse hepatocytes were isolated using the Liver Perfusion Kit mouse & rat (Miltenyi Biotec, 130-128-030) following the manufacturer's instructions. The lobus hepatis dexter was dissected, and subsequently perfused using the pre-programmed protocol 37C\_m\_LIPK\_1 via the gentleMACS Octo Dissociator system with heaters (MACS Technology, Miltenyi Biotec). The perfused liver lobe was homogenized via the gentleMACS program LIPK\_HR\_1. Enzymatic digestion was stopped by adding 5 ml attachment medium (Williams E media (Life Technologies, 22551089) supplemented with 2.24 g/l NaHCO<sub>3</sub>, 100 U/100  $\mu$ M penicillin/streptomycin, 100  $\mu$ M dexamethasone (Biozol, FBM-10-1134), 2 mM L-glutamine and 10% FCS). The cell suspension was filtered through a 100  $\mu$ m cell strainer. The gentleMACS C tube and the cell strainer were subsequently rinsed twice with 4 ml of attachment medium.

Cells were collected via centrifugation (5 min, 77 xg, 4°C). The supernatant was discarded and the pellet was washed twice with ice-cold PBS. 10<sup>6</sup> cells were seeded into each well of a 6-well plate in attachment medium. After 3 h, the medium was changed and cells were cultured in 5% CO<sub>2</sub> at 37°C using Williams E media supplemented with 2.24 g/l NaHCO<sub>3</sub>, 100 U/100  $\mu$ M penicillin/streptomycin, 100  $\mu$ M dexamethasone and 2 mM L-glutamine. Hepatocytes were treated with 100  $\mu$ M BA (Cayman Chemical Company, 26409) or 0.21% DMSO (vehicle) for 48 h prior to analysis. BA was added directly to the medium without any conjugation.

### siRNA mediated knockdowns

Knockdowns were performed using siRNA from Horizon Discovery: *Ppara*: ON-TARGETplus Mouse *Ppara* siRNA (Horizon, L-040740-01-0005); *Slc27a2*: ON-TARGETplus Mouse *Slc27a2* siRNA (Horizon, L-048371-01-0005); control: ON-TARGETplus Non-targeting Pool (Horizon, D-001810-10-05). For transfection, 25 nM of target siRNA was mixed with OptiMEM, and separately a mixture of Lipofectamine RNAiMAX (Invitrogen, 13778-030) and OptiMEM was prepared. The two mixtures (siRNA + OptiMEM; RNAiMAX + OptiMEM) were incubated for 5 min at room temperature. Then, the two mixtures were combined and incubated for another 5 min before adding to cultured primary mouse hepatocytes. Six hours after the addition of siRNA, the media was changed, and hepatocytes were treated with BA or vehicle. Hepatocytes were harvested and analysed 48 h later.

### Immunoblotting

Proteins were separated by running an SDS-PAGE with a 4-12% Tris NuPAGE gel (Thermo Scientific, NP0321PK2) or 12% home-made gels in MES buffer (Invitrogen, NP0002). Proteins were transferred from gels to a 0.2  $\mu$ m PVDF transfer membrane (Thermo Scientific, 88520) for 80 min at 350 mA. Membranes were blocked with 5% milk (Carl Roth, T145.5) diluted in PBS-T (1x PBS supplemented with 0.3% Tween 20 (Carl Roth, 9127.2)) for 1 h and incubated overnight with primary antibodies diluted in 5% milk in PBS-T: PPAR $\alpha$  (Abcam, ab126285) 1:1000, His-tag-HRP (Santa Cruz, sc-8036) 1:1000, and GAPDH (ThermoFisher, A300-641A) 1:2000. Membranes were washed three times with PBS-T at room temperature and incubated with the peroxidase conjugated anti-rabbit antibody (GE healthcare, GENA934, 1:5000) in 5% milk for 1 h at room temperature. Signal detection was performed with the SuperSignal West Femto Maximum Sensitivity Substrate (Thermo Fisher Scientific, 34094) on the G:Box Chemi-XX9 instrument (SynGene, 34397).

### RNA Sequencing

RNA from hepatocytes or livers was isolated using the RNeasy Mini Kit (Qiagen, 74104). RNA quality was analyzed and quantified via the Bioanalyzer (Agilent). Libraries were prepared using the NEBNext Ultra II RNA Library Prep Kit (New England Biolabs GmbH, Germany) according to the manufacturer's protocol. The quantity and quality of the libraries were assessed by BioAnalyzer (Agilent). Generated libraries were sequenced on an Illumina NovaSeq instrument with around 35 million reads per library (100 bp, paired-end).

### Sequencing data pre-processing

Trimming of sequencing adapters was performed with Trim Galore v.0.6.10 (Babraham Bioinformatics).<sup>16</sup> Low quality base pairs with a Phred score inferior to 20 were removed. RNA-seq reads were mapped to the primary assembly genomes provided by GENCODE (mm10, hg38)<sup>30</sup> using the splice-aware aligner STAR v.2.7.10b.<sup>17</sup> Mappable proportion of the genome was computed by using fa-Count v.377, reads with mapping quality <30 and PCR duplicates were discarded by using the samtools<sup>18</sup> suite v.1.3 and MarkDuplicates v.2.27.4 (Picard) (<https://broadinstitute.github.io/picard>). Expression levels were evaluated by assigning aligned reads to specific genomic features using featureCounts without allowing multimapping.<sup>31</sup> Strandness was determined by RSeQC.<sup>19</sup> Quality metrics report was generated using MultiQC.<sup>20</sup>

### Differential gene expression and gene set enrichment analyses

Features with a read counts sum inferior to 10 were discarded from analyses. Normalization and differential genes expression analysis was performed using DESeq2<sup>21</sup> (v1.36.0). To enhance stability and interpretability of estimates, shrinkage estimation for dispersions and fold changes was integrated, utilizing the *apeglm* R package. Fold changes were shrunk with the *apeglm* method<sup>23</sup> (v.1.12.0). Genes set enrichment analyses were performed on differentially expressed genes based on the adjusted p-values below 0.05 and an absolute log<sub>2</sub> fold change greater than 0.5 using the enrichR<sup>22</sup> platform.

### Thermal shift assay

The thermal shift assay was performed using the Applied Biosystems Protein Thermal Shift kit (Thermo Fisher Scientific, 4461146) according to the manufacturer's instructions. For each test, 3  $\mu$ l of human PPAR $\alpha$  protein (Thermo Fisher Scientific, PV4692) was

used. The ligand, BA (Cayman Chemical Company, 26409), was tested at four different concentrations: 500  $\mu$ M, 100  $\mu$ M, 10  $\mu$ M, and 1  $\mu$ M. Protein melt reactions were carried out using the QuantStudio 6 Pro Real-Time PCR System, and data analysis was performed using the  $\Delta$ Tm-Derivative method as recommended by the manufacturer.

### Fatty Acid Oxidation (FAO) Assay

Fatty acid oxidation activity was measured using the Fatty Acid Oxidation Assay Kit (Assay Genie, SKU: BR00001), according to the manufacturer's instructions. In brief, primary mouse hepatocytes were seeded in 6-well plates at a density of  $1 \times 10^6$  cells per well. Cells were transfected with 25 nM *Ppara* siRNA or control siRNA. Six hours later, the medium was changed and hepatocytes treated with 100  $\mu$ M BA, 500 nM GW7647 (Sigma-Aldrich, G6793), or DMSO for 48 h. Primary mouse hepatocytes were then incubated with the assay reagents for 60 min, and the optical density at 492 nm (OD 492nm) was measured using a microplate reader. The  $\Delta$ OD values were used to calculate enzyme activity according to the kit manual. Data were normalized to protein concentration, which was determined by the BCA assay.

### TR-FRET Peroxisome Proliferator Receptor alpha Coactivator Assay

The TR-FRET Peroxisome Proliferator Receptor alpha (PPAR $\alpha$ ) Coactivator assay was performed using the LanthaScreen TR-FRET PPAR $\alpha$  Coactivator Assay Kit (Thermo Fisher Scientific, PV4684) according to the manufacturer's instructions. BA was tested at five concentrations: 500  $\mu$ M, 250  $\mu$ M, 100  $\mu$ M, 10  $\mu$ M and 1  $\mu$ M. After adding the assay reagents, the 96-well plate was incubated for 1 h at room temperature. Fluorescence was measured using a microplate reader with excitation at 340 nm and emission at 520 nm and 495 nm. Data analysis was performed by calculating the TR-FRET ratio (emission at 520 nm/emission at 495 nm).

### Luciferase Assay

The luciferase assay was performed using the Firefly/Renilla Dual Luciferase Assay (Sigma Aldrich, SCT152) according to the manufacturer's instructions. Primary mouse hepatocytes (PMH) were seeded in 24-well plates at a density of  $2.4 \times 10^5$  cells/well in 500  $\mu$ l growth medium. The next day, cells were transfected with 400 ng *Acaa1b* promoter or PPRE firefly reporter plasmid (Addgene, 1015), and 40 ng Renilla control plasmid (pGL4.74) using the Lipofectamine 3000 Transfection Reagent (Invitrogen, L3000008). After 6 h, media was changed and cells were treated with 100  $\mu$ M BA, 500 nM GW7647, or 0.21% DMSO (vehicle) for 48 h. Cells were lysed according to the kit manual. Firefly and Renilla luciferase activity were measured using a luminometer. Firefly signal was normalized to Renilla signal for each sample.

The PPRE X3-TK-Luc was a gift from Bruce Spiegelman (Addgene plasmid 1015).<sup>32</sup>

### PPAR $\alpha$ expression and purification

Human wildtype PPAR $\alpha$  (amino acids 200–468 with N-terminal 6xHis-tag) was expressed in *E. coli* BL21 Rosetta2, as previously described.<sup>10</sup> Briefly, bacteria were cultured in TB medium (12 g/L Trypton, 24 g/L yeast extract, 0.4% Glycerol, 0.017 M KH<sub>2</sub>PO<sub>4</sub>, 0.072 M K<sub>2</sub>HPO<sub>4</sub>, 30  $\mu$ g/ml kanamycin, 34  $\mu$ g/ml chloramphenicol) overnight at 37°C. This culture volume was increased step-wise and maintained at 30°C. For protein expression, the temperature was reduced to 15°C, and 2 h later, 0.5 mM isopropyl b-D-galactopyranoside was added. Bacteria were harvested and resuspended in 40 ml lysis buffer (20 mM Tris-HCl pH 8, 150 mM NaCl, 1 mM TCEP-HCl, 10% glycerol, 5 mM MgCl<sub>2</sub>, DNase, and 1 tablet protease inhibitor complex (Sigma-Aldrich, 11836145001)). Lysis was performed by sonicating 5 times for 2 min on a Branson 250 sonicator on ice. The lysate was centrifuged for 30 min, 80,000 xg, 4°C and imidazole was added to a final concentration of 10 mM.

Recombinant PPAR $\alpha$  protein was isolated from bacterial lysates by immobilized metal-ion affinity chromatography (IMAC) using a HiTrap-chelating column on an ÄKTA pure25 system (Cytiva, Marlborough, MA, USA). The column was equilibrated and washed with binding buffer (containing 20 mM Tris-HCl, 150 mM NaCl, 10 mM imidazole, and 1 mM TCEP, pH 8.0), followed by gradient elution up to 500 mM imidazole. Protein-containing fractions were pooled and further purified to homogeneity by size exclusion chromatography (SEC) on a Superdex 200 Increase 10/300GL column (Cytiva) using imidazole-free binding buffer. Protein integrity, identity and purity were confirmed by SDS-PAGE and Western blot.

### Coomassie staining

Coomassie staining solution was prepared by dissolving 70 mg Brilliant Blue G-250 (BioRad, 1610406) in 1 L distilled water and adding 3 ml of 30 mM HCl. Following electrophoresis, gels were washed three times with distilled water and incubated with the staining solution for 30 min at room temperature. After adding the staining solution, gels were heated for 10 sec in a microwave. After staining for 30 min, gels were washed using distilled water. Representative images were taken with the GelDoc Go imaging system (BioRad).

### Crystal Structure Determination

For co-crystallization of PPAR $\alpha$  with BA and the PGC-1 $\alpha$  peptide, approximately 400 different crystallization conditions were screened in 96-well plates using sitting-drop vapor diffusion method. The crystallization drops with 200 nl final volume size (sample and reservoir mixed in equal volumes) were set with a Mosquito Xtal3 pipetting robot (SPT Labtech, Melbourn, England). For this screening, the protein was concentrated to 11 mg/mL in SEC buffer (20 mM TrisHCl, pH 8.0, 150 mM NaCl and 1 mM TCEP-HCl) and mixed with 1 mM PGC-1 $\alpha$  peptide (QEAEPSLLKKLLAPANT) and 20 mM BA. Precipitated BA was removed by centrifugation. Crystals grew at 19°C in a condition containing 20% (w/v) PEG 3350 and 0.2 M Na<sub>2</sub>HPO<sub>4</sub> as reservoir buffer. Crystals appeared after

one day and grew to their final size of 100–500  $\mu$ m within 3 days. A crystal was transferred to a cryo-buffer containing 13% glycerol (v/v) in the reservoir solution and flash-frozen in liquid nitrogen. X-ray diffraction data were collected at 100 K at EMBL beamline P14 at the DESY synchrotron in Hamburg, Germany. The diffraction data were indexed, integrated and scaled with XDS<sup>24</sup> and STARANISO<sup>25</sup> as implemented in ISPyB<sup>26</sup> at DESY. The structure PDB ID 1k7I<sup>33,34</sup> was used as search model for molecular replacement (MR). Two protein chains are present in the asymmetric unit of the crystals and the inhibitor was refined with full occupancy in both chains. Phenix<sup>27</sup> was used for refinement and Coot<sup>28</sup> for model building. Stereochemical restraints for ligand refinement were generated using grade2 (<https://grade.globalphasing.org>). Molecular figures were prepared using PyMOL (<https://pymol.org>). The crystal structure has been deposited in the protein databank with PDB: 9T5S.

## QUANTIFICATION AND STATISTICAL ANALYSIS

Data are presented as mean  $\pm$  standard error of the mean (SEM). Statistical significance of data was tested using a two-tailed Student's t-test when comparing two groups. Statistical analyses were undertaken in GraphPad Prism software v8.0. p values < 0.05 were considered statistically significant. Information on replicates for each experiment is provided in the figure legends.

## Supplemental information

### **Bempedoic acid directly binds and activates PPAR $\alpha$**

**Christina Papa, Alina Rose, Hugo N.G. Martin, Abibe Useini, Florian Geier, Longsheng Liao, Jesús Rafael Rodríguez-Aguilera, Philipp Valina-Allo, Anne Hoffmann, Andrey Tvardovskiy, Faiqa Zulfqar, Andrea Zimmerman, Gerda Schicht, Fritzi Ott, Christiane Körner, Beatrice Engelmann, Ulrike Rolle-Kampczyk, Martin von Bergen, Matthias Meier, Till Bartke, Daniel Seehofer, Nora Klöting, Madlen Matz-Soja, Georg Damm, Jes-Niels Boeckel, Joerg M. Buescher, Matthias Blüher, Ulrich Laufs, Olga Bondareva, Norbert Sträter, Georg Künze, John T. Heiker, and Bilal N. Sheikh**

**Supplemental Material to:**

## **Bempedoic acid directly binds and activates PPAR $\alpha$**

Christina Papa, Alina Rose, Hugo N. G. Martin, Abibe Useini, Florian Geier, Longsheng Liao, Jesús Rafael Rodríguez-Aguilera, Philipp Valina-Allo, Anne Hoffmann, Andrey Tvardovskiy, Faiqa Zulfqar, Andrea Zimmerman, Gerda Schicht, Fritz Ott, Christiane Körner, Beatrice Engelman, Ulrike Rolle-Kampczyk, Martin von Bergen, Matthias Meier, Till Bartke, Daniel Seehofer, Nora Klöting, Madlen Matz-Soja, Georg Damm, Jes-Niels Boeckel, Joerg M. Buescher, Matthias Blüher, Ulrich Laufs, Olga Bondareva, Norbert Sträter, Georg Künze, John T. Heiker and Bilal N. Sheikh

## Supplemental Figures

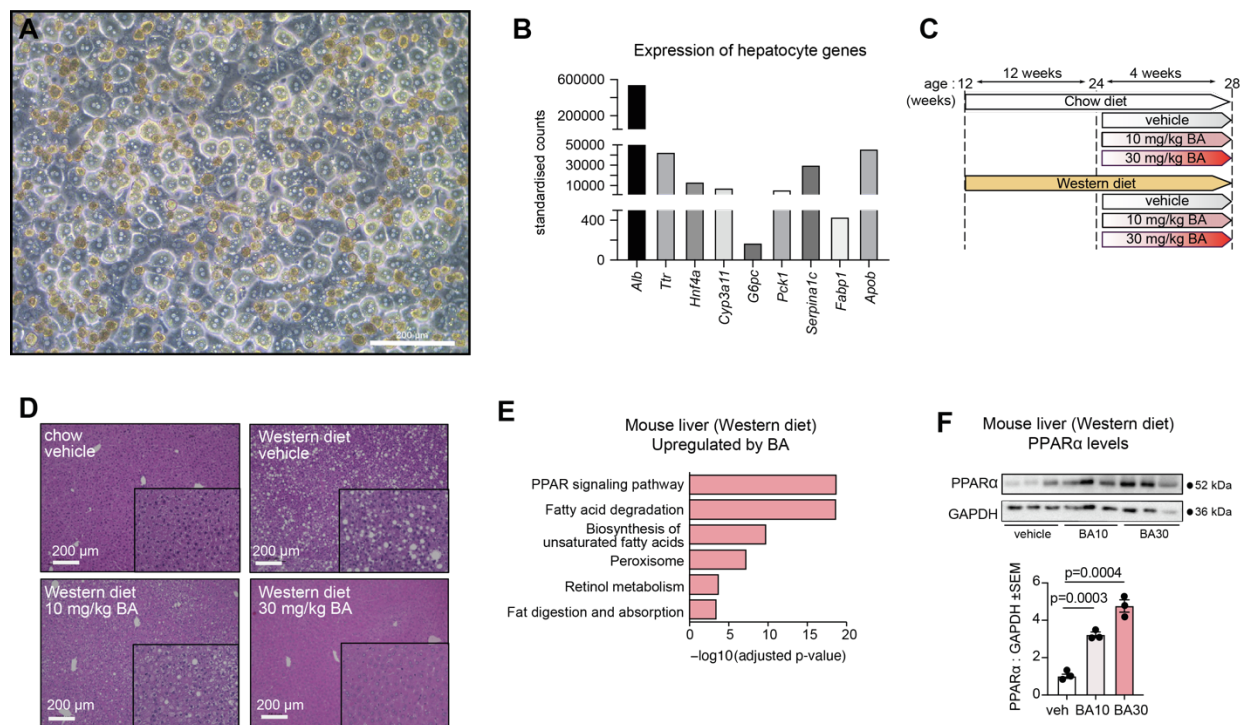


**Figure S1 – Bempedoic acid activates PPAR $\alpha$**

Related to Figure 1

(A) Exemplary image of primary mouse hepatocytes used in this study. Bi-nucleated hepatocytes were commonly observed. Scale bar equals 200  $\mu$ m.

(B) Expression of genes typically used as markers of primary mouse hepatocyte [S1,S2]. Data were extracted from RNA-seq analyses of primary mouse hepatocytes, and are averaged across 8 biological replicates. The normalized expression levels are provided, which standardizes for overall sequencing depth.

(C) Experimental design of the in vivo study. Male C57BL/6N mice were fed with chow or Western diet for 12 weeks. Randomized animals under different diets were grouped to receive either vehicle, 10 mg/kg body weight BA (BA10) or 30 mg/kg body weight BA (BA30) daily via oral gavage. After 4 weeks of diet and treatment, animals were sacrificed and livers were collected for further analysis.

(D) Histology of livers from chow and Western diet-fed animals treated with vehicle, BA10 and BA30. Western diet: n = 6 animals per group; chow: n = 5 animals per group.

(E) KEGG-annotated pathways significantly upregulated in livers of Western diet-fed mice treated with BA30. List of significantly upregulated genes (Benjamini-Hochberg adjusted p-value < 0.05, log2 fold change > 0.5) was used for these analyses. n = 4 mice per group.

(F) Top: Western blot for PPAR $\alpha$  and GAPDH proteins following BA treatment of Western diet-fed mice. Bottom: Signal quantification analysis of PPAR $\alpha$  : GAPDH signal. Data are provided as mean  $\pm$  SEM, and were analysed via a two-tailed Student's t-test. n = 3 animals per group.

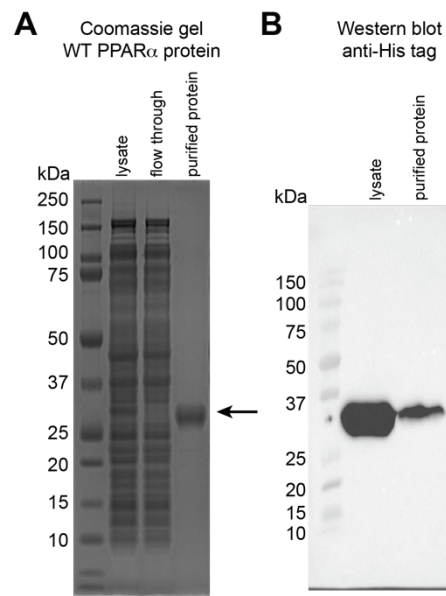


**Figure S2 – Expression and purification of the ligand binding domain of PPAR $\alpha$**

Related to Figure 2

(A) Coomassie-stained gel showing the initial bacterial lysate, the flow through from the Ni<sub>2</sub>NTA column, and the purified protein following size-exclusion chromatography.

(B) Western blot using antibodies raised against the His-tag.

## Supplemental References

- S1. Ardisasmita, A.I., Schene, I.F., Joore, I.P., Kok, G., Hendriks, D., Artegiani, B., Mokry, M., Nieuwenhuis, E.E.S., and Fuchs, S.A. (2022). A comprehensive transcriptomic comparison of hepatocyte model systems improves selection of models for experimental use. *Commun Biol* 5, 1094. [10.1038/s42003-022-04046-9](https://doi.org/10.1038/s42003-022-04046-9).
- S2. Franzen, O., Gan, L.M., and Bjorkegren, J.L.M. (2019). PanglaoDB: a web server for exploration of mouse and human single-cell RNA sequencing data. *Database (Oxford)* 2019. [10.1093/database/baz046](https://doi.org/10.1093/database/baz046).